Variations in recorded acoustic gunshot waveforms generated by small firearms

Steven D. Beck, Hirotaka Nakasone, and Kenneth W. Marr

Citation: The Journal of the Acoustical Society of America **129**, 1748 (2011); doi: 10.1121/1.3557045
View online: https://doi.org/10.1121/1.3557045
View Table of Contents: https://asa.scitation.org/toc/jas/129/4
Published by the Acoustical Society of America

Variations in recorded acoustic gunshot waveforms generated by small firearms

Steven D. Beck[a)]
BAE Systems, 6400 Tracor Lane 27-16, Austin, Texas 78725

Hirotaka Nakasone and Kenneth W. Marr
Federal Bureau of Investigation, Building 27958A, Quantico, Virginia 22135

(Received 7 May 2010; revised 8 November 2010; accepted 24 January 2011)

Analysis of recorded acoustic gunshot signals to determine firearm waveform characteristics requires an understanding of the impulsive signal events, how the waveforms vary among different sources, and how the waveforms are affected by the environment and the recording system. This paper presents empirical results from waveforms produced by different small firearms and an analysis of their variations under different and controlled conditions. Acoustic signals were generated using multiple firearm makes and models firing different ammunition types. Simultaneous recordings from the microphones located at different distances from the source and at different azimuth angles (from the line-of-fire) were used to study source characteristics and sound propagation effects. The results indicate that recorded gunshot waveforms generally consist of multiple acoustic events, and these are observable depending on the received distance and azimuth angle. The source blast size, microphone distance, and microphone azimuth angle are the primary factors affecting the recorded muzzle blast characteristics. Ground or object reflections and ballistic shockwaves and their reflections can interfere with the muzzle blast waveform and its measurements. This experiment confirmed and quantified the wide range of correlation results between waveforms recorded from different source, microphone distance, and microphone angle configurations.
 [DOI: 10.1121/1.3557045]

PACS number(s): 43.28.Mw, 43.28.Gq [DKW] Pages: 1748–1759

I. INTRODUCTION

Acoustic gunshot detection and recording systems are increasingly being used by the forensic, surveillance, and military communities. Gunshot detection systems are used by law enforcement for automatic surveillance and generally consist of an array of microphones deployed around city blocks and are connected to a central computer system.[1,2] These systems detect gunshot-like events from each microphone and use time-of-arrival and triangulation techniques to localize the sound source, with a primary goal of improving the police response time to investigate the event. The audio quality of these surveillance systems is limited by telephone bandwidth restrictions and microphone design. Sniper detection systems used by the military are usually small microphone arrays that are mounted on soldiers or vehicles.[3–7] These systems are designed to detect gunshot muzzle blasts and ballistic shockwaves and rapidly localize the shooter's position in azimuth (angle), range (distance), and elevation (height). In order to pinpoint the shooter location, the detected muzzle blast from the weapon is used to calculate the angle of arrival relative to the array orientation, and the array measurements of the ballistic shockwave are used to estimate the range to the shooter.

In forensic applications, the Federal Bureau of Investigation (FBI) receives many evidential acoustic recordings that potentially contain gunshot sounds. Often these recordings were captured by a single microphone system recorded by the police 911 Emergency Call Center, by personal recording equipment, or from a body recorder worn by an undercover agent. These audio recordings have numerous unknown factors that can prevent analysts from reaching a conclusive determination about any potential gunshot event. The most salient perceptual cues about gunshot sounds in a recording include a relatively loud and sharp impulsive signal often trailed by reverberations and echoes. However, these perceptual cues do not necessarily lead to quantitative proof of existence of the gunshot nor do they necessarily help to determine the weapon and ammunition types. Typical forensic questions regarding these recordings include:

(1) Are the perceived impulse sounds generated by a gun fired at the scene?
(2) How many shots were fired?
(3) How many weapons were involved?
(4) Which shot was fired by a particular weapon?

There are numerous factors affecting the basic acoustic characteristics of a gunshot wave and the resulting shape of the recorded signal.[8,9] An earlier study addressed the effect of high intensity gunshot sounds on acoustic sensors and recording equipment.[10] These results showed high correlations between multiple shots fired from the same weapon that used similar sensor/recording systems, but poor correlations between shots fired from the same weapon at different ranges and firing directions relative to the microphone. The same study also reported that different microphones and recording systems caused significant changes to the waveform

[a)]Author to whom correspondence should be addressed. Electronic mail: steve.beck@baesystems.com

 0001-4966/2011/129(4)/1748/12/$30.00

shape of shots fired by the same weapon from the same firing and recording configurations.

The scope of this new investigation was limited to the analysis of waveform characteristics measured from time series gunshot signals obtained from high-quality recordings. The experiment used simultaneous recordings from microphones arranged in multiple configurations (range and azimuth) and was designed to capture variations in the signal due to differences in the sources and differences in the spatial sound propagation paths. Section II provides an overview of sound generation from small firearms and the sources of variation in the recorded waveforms. Section III describes the equipment and experimental procedures used in the gunshot recording experiment. Section IV shows empirical examples of waveform variations due to the source, propagation, and receiving conditions, with the results summarized in Sec. V. Since many firearm manufacturers list the caliber, barrel length, and bullet weight measurements in British units, both British and SI units are used where appropriate.

II. FIREARM SOUND GENERATION AND PROPAGATION

Multiple sounds are generated and radiate through the air when a firearm is discharged. These sounds are produced by internal mechanisms that occur before the bullet exits the barrel, by the propellant gasses under very high pressure escaping as the bullet leaves the barrel (muzzle blast), by the supersonic bullet (ballistic) shockwave, and by reflections of these sounds from surfaces in the ray path. Reverberant acoustic energy normally dominates the signal a few milliseconds after the initial blast. Figure 1 illustrates the multiple sounds radiating from a revolver, along with the corresponding responses from microphones at different locations.

As illustrated in this figure, gunshot audio recordings have waveform shapes that vary significantly depending on the characteristic properties of the source and the location of the microphone relative to the sound sources. This section describes the relevant theory related to firearm sound generation and propagation and the expected variations due to different firearm-microphone recording configurations.

A. Internal ballistics

Internal ballistics is the study of the mechanical and chemical actions taking place inside a firearm during discharge. Descriptions of firearm internal ballistics and detailed mathematical models can be found in Ref. 11. The waveform shapes resulting from internal ballistic actions and the timing among these actions depend on factors such as the ammunition type and the weapon type, make, model, and barrel length. The goal in forensic gunshot waveform analysis is to find unique waveform shapes or a sequence of acoustic events for a given type of firearm that are repeatable and that correlate well with known examples or other recorded impulses.

During a firearm discharge and before the bullet exits the barrel, there are number of actions that produce sounds. Mechanical sounds from cocking, ratcheting, and hammer strikes have relatively low intensity and are generally not detectable. The primary internal sounds of interest include the

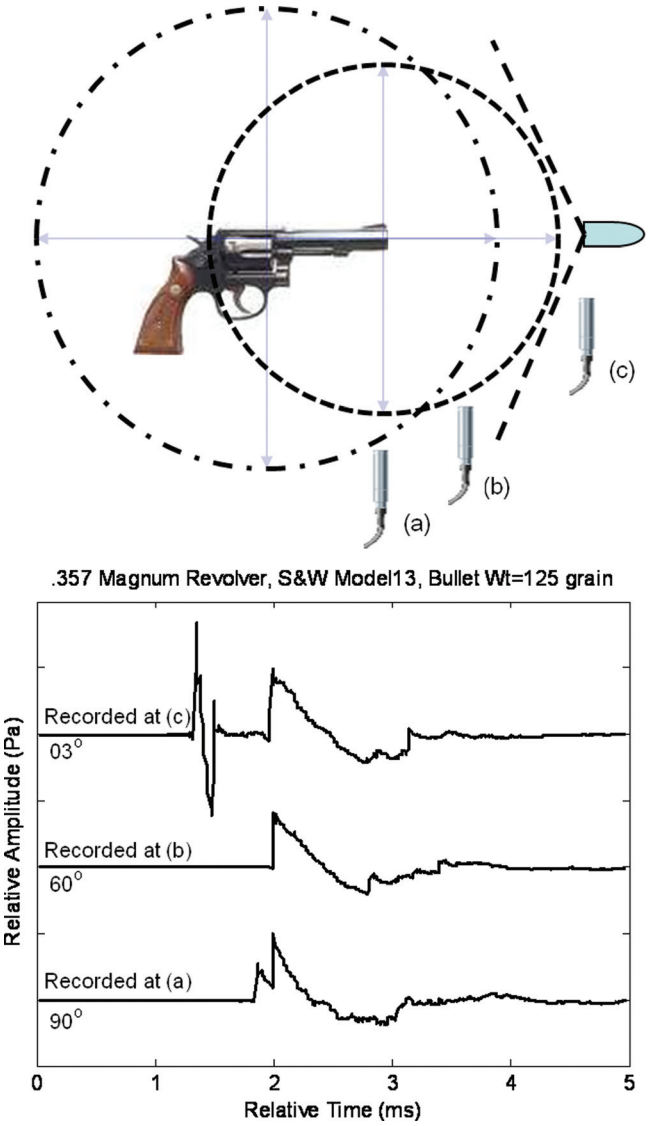

FIG. 1. (Color online) Variations in acoustic waveforms from a revolver firing a supersonic round—the microphone at (a) records the cylinder blast followed by the muzzle blast but no ballistic shockwave; the microphone at (b) records the muzzle blast but the cylinder blast and the ballistic shockwave are not distinguishable; and the microphone at (c) records the ballistic shockwave followed by the muzzle blast but the cylinder blast is not distinguishable.

primer explosion and leaks from gasses under high. For example, as a revolver is fired and the gunpowder burns, gasses under high pressure escape from the gap between the cylinder and the barrel, creating an explosive sound prior to the muzzle blast and causing a loss of pressure inside the barrel with a corresponding decrease in the bullet exit speed. Figure 2 shows a high speed photograph of a revolver shortly after being fired. The photograph shows the gas escaping from the cylinder gap and the gas in front of the bullet caused by the compressed propellant gasses expanding rapidly and accelerating to velocities greater than the exiting bullet (in this case an experimental double bullet).

B. The muzzle blast

The sound most often associated with a gunshot is the loud popping sound produced by the muzzle blast.

FIG. 2. (Color online) High speed photograph of a revolver showing gas explosions from the cylinder gap and the muzzle (photograph provided courtesy of the FBI).

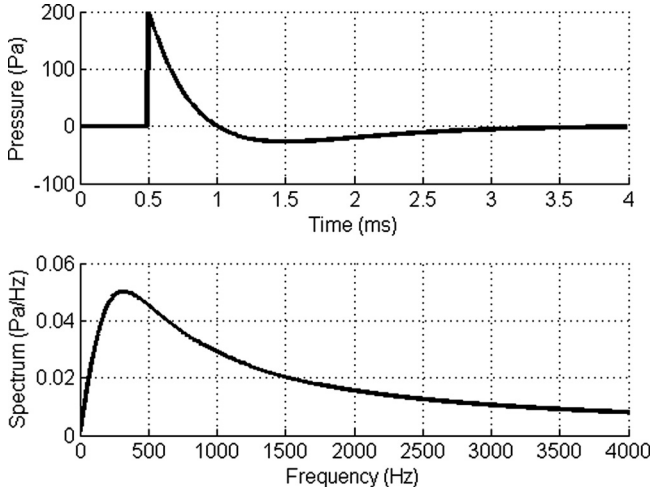

FIG. 3. The Friedlander model for an ideal small firearm muzzle blast and its analytic Fourier spectrum.

The muzzle blast is an explosive shockwave in air produced by propellant gasses under extremely high pressure that expand rapidly once the bullet exits the muzzle. Ideal explosions in air create shockwaves characterized by an almost instantaneous rise in pressure, followed by an exponential decay from the peak value to a partial vacuum, and then back to the ambient air pressure level. This general description of an explosion in air is used to characterize acoustic gunshot muzzle blasts. A detailed treatment of explosive shocks in air is given in Ref. 12.

The waveform features most commonly used to describe a muzzle blast (or any explosion in air) are the peak amplitude, the rise time, the positive phase duration, and the negative phase duration. The highest peak in the sound pressure wave is called the peak overpressure and denoted by P_s. The rise time is defined as the duration required for the sound pressure to rise from the ambient level P_0 to its peak level. The rise time of an explosive shock front has been measured at less than a microsecond in high speed recording system; however, it is usually much slower in audio recordings due to the front-end electronic low-pass filter (LPF) response of the recording system. The positive phase duration is the time period required for the pressure wave to go from peak overpressure back to the ambient level (the first zero crossing, where zero is the recorded ambient pressure level). The positive phase duration and the area under the curve during the positive phase are directly related to the size of the blast under ideal conditions. Finally, the negative phase duration is the time period where the sound pressure is below the ambient level. Ideally, the negative phase of the pressure wave asymptotically returns to the ambient level. In practice, the negative phase of recorded blast waves oscillates slowly around ambient as it decays due to inertia, aftershocks, and turbulence.

The expression most commonly used to model an explosion in air or a blast wave is the Friedlander equation (Ref. 12, p. 5)

$$p(t) = P_0 + P_s\left(1 - \frac{t}{T_0}\right)e^{-bt/T_0}, \tag{1}$$

where P_s is the peak overpressure, T_0 is the positive phase duration, and b is the rate of exponential decay. The top plot in Fig. 3 shows the pressure curve for a typical muzzle blast waveform generated using the Friedlander model with parameters $T_0 = 0.5$ ms and $b = 1$. For this example, the peak overpressure Ps was set to the value 200 Pa, indicating a sound pressure level (SPL) of 140 dB re 20 μPa.

The shape of a recorded blast wave and its model parameters Ps and T_0 are directly related to the size of the explosion. The actual blast size is a function of the firearm, the ammunition, and the internal ballistics. In general, there is a direct functional relationship between the blast size and the caliber of the firearm and inverse relationship with the bullet weight and length of the barrel, all other variables being equal. On the other hand, the bullet speed is directly related to the barrel length, but inversely related to its weight. The blast size is consistent for multiple shots under the same conditions, as will also be shown in Sec. IV using shot-to-shot waveform correlations.

C. Spectrum of the muzzle blast and variations due to filtering

The effects of the recording system can most easily be analyzed in the frequency domain using the Friedlander model. Starting with the Fourier transform pairs[13]

$$u(t)e^{-\alpha t} \leftrightarrow \frac{1}{\alpha + jw},$$
$$u(t)te^{-\alpha t} \leftrightarrow \frac{1}{(\alpha + jw)^2}, \tag{2}$$

where $u(t)$ is the unit step function, α is the decay rate (1/s), w is the angular frequency (rad/s), and j is the square root of -1. If we let $\alpha = b/T_0$, the Fourier transform of the Friedlander equation is

$$F(w) = \frac{P_s}{\alpha + jw} - \frac{P_s}{T_0(\alpha + jw)^2} = \frac{P_s((b-1) + jwT_0)}{T_0(\alpha + jw)^2}$$
$$= \frac{P_s}{T_0}\frac{(b-1) + jwT_0}{(b/T_0 + jw)^2}. \tag{3}$$

The magnitude of this Fourier transform is found by taking the magnitude of the numerator and the denominator

$$\|F(w)\| = \frac{P_s}{T_0}\frac{\sqrt{(b-1)^2+T_0{}^2w^2}}{(b/T_0)^2+w^2}. \quad (4)$$

The magnitude of the analytic spectrum using the parameter values previously defined for the Friedlander equation is shown in the bottom plot in Fig. 3. The peak in the spectrum is found by taking the derivative with respect to the frequency w and setting it equal to zero. The peak frequency is

$$w_{\text{peak}} = \frac{1}{T_0}\sqrt{-b^2+4b-2}. \quad (5)$$

For example, with $T_0 = 0.5$ ms and $b = 1$, the peak frequency $f_{\text{peak}} = 2000/(2\pi) = 318$ Hz. The radicand has two real roots, and w_{peak} is defined for values of the slope parameter b in the range of $2\pm\sqrt{2}$. For the small firearms used in this study, the value of b was empirically measured to be close to 1.

Filtering modifies the energy spectral density, causing variations in the signal waveform. Most audio recording systems contain a LPF used to attenuate the high frequency signals and prevent aliasing in digitized systems. Voice recorders commonly have a LPF cutoff frequency around 4000 Hz, and audio compact disk audio has a cutoff frequency around 22 kHz. Audio systems also use high pass filters (HPFs) to attenuate low frequencies including direct current, with typical cutoff frequencies between 50 and 100 Hz. Telephone channels contain bandpass filters that limit frequency content of the signals between 300 and 3200 Hz. Low-pass filtering attenuates the high frequency energy of the blast, primarily distorting the rise time and peak overpressure. High pass filtering attenuates the low frequency energy components of the blast causing significant waveform distortion of the slope, the positive phase duration, and the negative phase of the signal.

D. Muzzle blast waveform variations due to blast size, distance, and azimuth angle

A spherical charge will produce an explosion that expands spherically in a homogeneous medium. In this case, acoustic waveform parameters scale with respect to the cube root of the blast size as measured by the energy or the charge weight. This cube root scaling is known as Hopkinson's scaling laws (Ref. 12, Chap. 3) ANSI Standard S2.20-1983 in Refs. 14 and 15 gives equations for the pressure, positive phase duration, and impulse of an explosion as functions of the distance scaled by the cube root of the charge weight. In forensic applications, the charge weight is unknown, so scaling is accomplished using the muzzle blast energy size E. According to the scaling laws, two explosions will have the same observed pressure P under the same atmospheric conditions when the following relationships hold:

$$\frac{E_2^{1/3}}{E_1^{1/3}} = \frac{R_2}{R_1} = \frac{T_2}{T_1} = \frac{I_2}{I_1}, \quad (6)$$

where R is the distance, T is the positive phase duration, and I is the impulse. For example, an explosion with energy E produces a pressure P at range R from the source, and a waveform with positive phase duration T and impulse I. Another similar explosion of size $K^3 \cdot E$ will produce a pressure P at range $K \cdot R$ with positive phase duration $K \cdot T$ and impulse $K \cdot I$. Therefore, a second explosion eight times greater than the first would produce the same pressure at twice the distance, with double the positive phase duration and impulse.

Although they are axi-symmetric about the line-of-fire, muzzle blasts differ from conventional explosions in air because they are not spherically symmetric. The peak overpressure of the muzzle blast scales as a function of the angle of the microphone location relative to the line-of-fire. One proposed model for the angular peak overpressure is

$$P(\theta) = P_{0^\circ}\left(1 - \frac{P_{0^\circ} - P_{180^\circ}}{P_{0^\circ}}\sin\left(\frac{\theta}{2}\right)\right), \quad (7)$$

where θ is the angle with respect to the line-of-fire, also known as the azimuth angle, P_{0° is the peak forward pressure and P_{180° is the peak pressure behind the firearm. Figure 4 shows a plot of this model for a hunting rifle with $P_{0^\circ} = 112$ Pa and $P_{180^\circ} = 75$ Pa. The calibrated peak pressures from two shots recorded at various angles and at 30 m from the source are relatively close to the model estimated pressures, but deviate because the rear pressures are attenuated due to the presence of the shooter's body.

E. Acoustic and shockwave propagation

The propagation of an acoustic wave through the atmosphere is well understood.[16,17] In the absence of spherical spreading and absorption, the shape of the acoustic wave does not change as it propagates. Spherical spreading causes a $1/R^2$ loss in sound intensity (a 6 dB loss per doubling of the distance). Molecular absorption converts sound energy into heat energy as the wave propagates, causing attenuation with a strong dependence on frequency. In the region from 1 to 2 m above the surface of the ground, additional waveform distortions are caused by wind and temperature gradients.

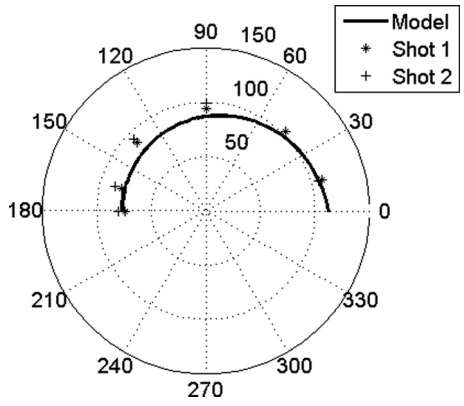

FIG. 4. Angular model of the muzzle blast peak overpressure and the peak overpressures from two calibrated recordings made at multiple angles with respect to the line of fire.

Given information regarding the geometries involved and the meteorological conditions, acoustic waves are predictable and obey the laws of linear systems theory.

Shockwaves differ from acoustic waves in that they move faster than the speed of sound, have non-zero particle velocities and displacements, and contain large and almost instantaneous jumps in their parameters (temperature, pressure, and density) across the wavefront. A detailed derivation of the non-linear wave equation is given in Ref. 18 and for muzzle blasts in air in Ref. 12. For a non-linear wave, the propagation speed v differs from that of an acoustic wave and depends on the instantaneous amplitude of the signal[19]

$$v = v_0 + \beta u, \tag{8}$$

where u is the particle velocity and β is the coefficient of non-linearity in a fluid medium. In contrast, each point on a linear acoustic waveform ideally travels at the speed of sound v_0 for that medium, and the value of u approaches zero for linear acoustics. The coefficient of non-linearity for a specific medium is expressed as

$$\beta = \frac{1+\gamma}{2}, \tag{9}$$

where γ is the ratio of specific heats for that medium (ratio of the specific heat of the medium at a constant pressure to that of the medium at constant volume, where $\gamma = 1.4$ in standard air). The Mach number M_a is then expressed as

$$M_a = \frac{u}{v_0}, \tag{10}$$

where Mach 1 occurs when the wavefront of the medium is moving at the same speed as the speed of sound.

If the particle velocity $u > 0$, then the positive amplitude regions of the wave will travel faster than v_0 and arrive successively sooner than an acoustic wave. Likewise, the negative regions will travel slower than v_0 and arrive successively later. As the wave propagates it becomes more and more distorted until it shocks up. As the shockwave continues to propagate over distance, the positive and negative regions continue to spread by increasing their positive and negative phase durations—a process known as non-linear dispersion.

F. Ground reflections

In the majority of recordings from small firearms (especially from forensic conditions), both the weapon and the receiver microphone are located 1–2 m above a partially absorbing and partially reflecting surface, creating an echo from each source that can interfere with the muzzle blast waveform. Typical surfaces include grass-covered ground, pavement, or indoor floor materials. If we assume an acoustic point source and a far field wave (source distance far enough away to assume a plane wave) incident at the reflection surface, then the reflected wave will also be planar and the sound will reach the receiver via the direct path and the reflected paths. For impulsive sounds like gunshots, the received waveform will contain the direct path sound followed by the reflection, where the timing is determined by the relative locations of the source, reflecting surface, and receiver.

For an acoustic wave, the refraction indices for the air above the surface for both the incident and reflected waves are the same. If h_1 is the height of the source above the surface, h_2 is the height of the microphone, and r_0 is the projected distance along the surface between the source and the microphone, then by simple geometry

$$r_1 = \frac{r_0 h_1}{h_1 + h_2} \quad \text{and} \quad r_2 = \frac{r_0 h_2}{h_1 + h_2}. \tag{11}$$

The distance d_1 from the source to the point of reflection on the surface, the distance d_2 from this point to the microphone, and the direct path distance d_0 are then

$$d_1 = \sqrt{h_1^2 + r_1^2}, \quad d_2 = \sqrt{h_2^2 + r_2^2}, \quad \text{and}$$
$$d_0 = \sqrt{r_0^2 + (h_1 - h_2)^2}. \tag{12}$$

The expected time difference of arrival is then

$$t_{\text{doa}} = \frac{d_1 + d_2 - d_0}{v_0}. \tag{13}$$

A useful approximation for the expected time difference of arrival is

$$t_{\text{doa}} = \frac{2 h_1 h_2}{v_0 r_0} \tag{14}$$

accurate to approximately 6% for a separation distance $r_0 \geq 2(h_1 + h_2)$.

The time difference of arrival can have a significant effect on the shape of the received gunshot waveform. For example, if the source and the microphone are collocated at a height of 1.5 m above ground (direct path distance equals zero) and the speed of sound in air is 344 m/s, then the time difference between the direct path and vertically reflected path waves will be $2(1.5)/344 = 8.7$ ms. If a typical gunshot waveform has a 0.5 ms positive phase duration and a 2.5 ms negative phase, then the reflecting wave will not interfere with the direct path waveform. If the source and microphone separation distance is 30 m, then the time difference of arrival of the wavefronts will be 0.4 ms, and the direct path and reflecting field waveforms will be superimposed and interfere with each other. A more detailed description of reflected acoustic waves is described in Ref. 16.

III. GUNSHOT EXPERIMENT AND DATA COLLECTION

A gunshot data collection experiment was conducted at an outdoor range in Austin, TX, on August 16, 1997. The purpose of this experiment was to determine acoustic source and propagation channel characteristics that can affect recorded gunshot waveforms. The approach was to collect high-quality data while varying the acoustic sources and the direct paths in

a controlled procedure. Variations in the acoustic sources included multiple weapon types, weapon models, barrel lengths, ammunition, and bullet types. Variations in the propagation channel included different ranges and azimuth angles. Measurements of these variations were made from data simultaneously recorded from multiple microphone configurations.

A. Recording system equipment

The primary sensors used in this experiment were four B&K model 4136 microphones (Brüel and Kjær Sound and Vibration Measurements A/S, Nærum, Denmark). The B&K 4136 microphone was chosen for sensing acoustic gunshot waves because it has low sensitivity (1.6 mV/Pa), wide frequency range (flat from 4 Hz to 70 kHz), and wide dynamic range (open circuit distortion limit greater than 172 dB). The B&K 4136 is a pressure response microphone that measures the SPL at the diaphragm, but can measure the free-field response if the microphone diaphragm is positioned perpendicular to the direction of sound propagation. B&K model 2669L microphone preamplifiers were used, along with B&K 2690 A OS4 4-channel microphone signal conditioning units. The B&K microphone was mounted vertically on a tripod with the diaphragm 1.5 m (5 ft) above the ground. Microphone diaphragms oriented along the acoustic grazing angle have accurate free-field time-waveform histories; whereas microphones pointed at the source have a reflected wave from the diaphragm resulting in a peak pressure overshoot error up to 6 dB in Ref. 20.

The gunshot signals were digitized simultaneously and recorded using a 16-bit Teac RX800 8 mm wideband DAT recorder (Tokyo, Japan). This recorder was operated in the 8-channel 40 kHz bandwidth mode (sampled at 96 kHz per channel).

B. Test configurations

The gunshot data collection experiments were performed using four microphones arranged at multiple predetermined locations relative to the line-of-fire. Each test configuration was designed to separately measure the effects of distance or azimuth angle on the muzzle blast and the ballistic shockwave. Table I describes the multiple microphone configurations used for the data collection. Figure 5 shows a diagram of these configurations and a photograph of configuration #3 with microphones located at 3°, 30°, 60°, and 90° and at a constant distance of 3 m from the muzzle.

TABLE I. Recording configurations for different source-to-microphone distances (range) and different microphone location azimuth angles relative to the line-of-fire.

Configuration	Range (m)	Azimuth angle (deg)	Descr.
1	1.5, 3, 6, 30	3	Cross-range
2	1.5, 3, 6, 30	90	Cross-range
3	3	3, 30, 60, 90	Cross bearing
4	30	3, 30, 60, 90	Cross bearing
5	3	90, 120, 150, 180	Cross bearing
6	30	90, 120, 150, 180	Cross bearing

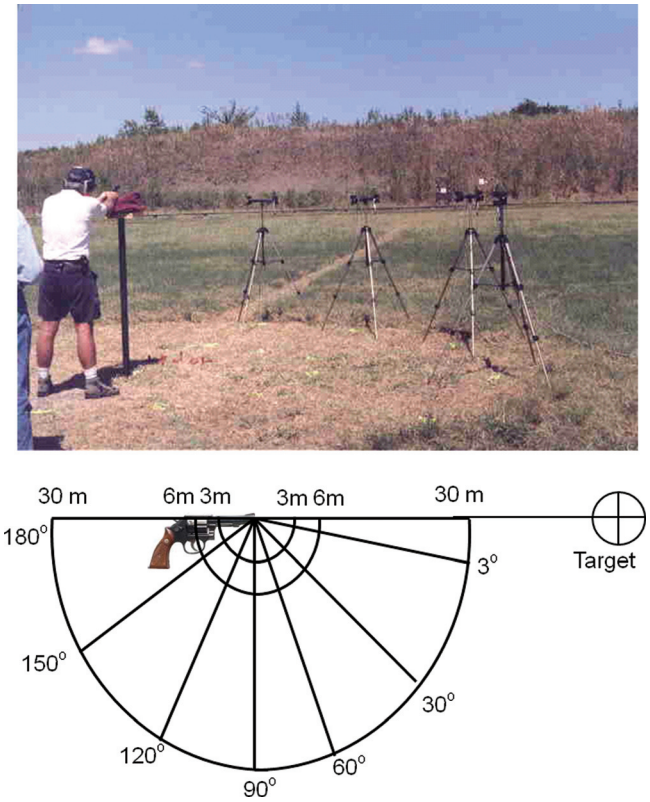

FIG. 5. (Color online) Data collection layout showing different microphone configurations and a photograph of configuration #3.

C. Weapons and ammunition

Small caliber firearms were used in this experiment that are commercially available and are of particular interest to law enforcement and for forensic applications. An index was assigned to each combination of firearm and ammunition type. The indices and the firearm type, caliber, manufacturer, model, barrel length, ammunition type, bullet weight, average bullet speed, and peak SPL are listed in Table II. The bullet weight is listed in both grains and grams, where a grain is 0.0648 g. These combinations were selected to provide a controlled set of experiments for comparing gunshot waveform characteristics according to the following conditions (from Table II):

(1) Effect of different firearm types—for example a 0.38 revolver (index #4) and a 9 mm semi-automatic pistol (index #6) with the similar barrel length were fired using similar ammunition.
(2) Effect of different firearm models—for example an S&W model 10 revolver (index #3) and model 60 revolver (index #5) were fired using the same ammunition.
(3) Effect of different barrel lengths—for example S&W model 10 .38 caliber revolvers with a 2.5 in. barrel (index #3) and a 4.0 in. barrel (index #4) were fired using the same ammunition.
(4) Effect of different ammunition types—the same weapons are fired with different ammunition types. Examples include ammunition with the same grain but different bullet type (indices #6 and #8), the same bullet type and different grain (indices #6 and #10), and different grain and different bullet type (indices #1 and #2).

TABLE II. Different firearms and ammunition types used in the data collection along with measured values of bullet speed and calculated values of peak SPL.

Index	Firearm caliber and type	Firearm make[a] and model	Barrel (in./cm)	Bullet type[b]	Bullet weight (grains/grams)	Bullet speed (m/s at 2 m)	SPL[c] (dB re 20 μPa)
1	0.357 Magnum revolver	S&W model 13	3.0/7.7	Win. STHP	145/9.4	362.4	155.4
2	0.357 Magnum revolver	S&W model 13	3.0/7.7	Rem. JHP	125/8.1	427.0	158.5
3	0.38 Revolver	S&W model 10	2.5/6.4	Win. STHP	110/7.1	269.7	153.0
4	0.38 Revolver	S&W model 10	4.0/10.3	Win. STHP	110/7.1	287.1	151.4
5	0.38 Revolver	S&W model 60	2.5/6.4	Win. STHP	110/7.1	250.2	155.4
6	9 mm Pistol	Sig Sauer P-226	4.5/11.5	Win. FMJ	115/7.5	333.8	153.7
7	9 mm Pistol	Colt model 2000	4.5/11.5	Win. FMJ	115/7.5	345.0	153.7
8	9 mm Pistol	Sig Sauer P-226	4.5/11.5	Win. STHP	115/7.5	344.7	152.5
9	9 mm Pistol	Colt model 2000	4.5/11.5	Win. STHP	115/7.5	357.5	153.1
10	9 mm Pistol	Sig Sauer P-226	4.5/11.5	Win. FMJ	147/9.6	280.7	152.4
11	9mm Pistol	Colt model 2000	4.5/11.5	Win. FMJ	147/9.5	288.3	151.9
12	0.30–06 Rifle	Winchester 70	22.0/56.4	Win. Soft Pt.	125/8.1	889.1	160.8
13	0.30–06 Rifle	Winchester 70	22.0/56.4	Win. Soft Pt.	165/10.7	827.5	160.1
14	0.223 Rifle	Colt M16A1	21.0/ 53.8	Win. Hollow Pt.	64/4.1	803.8	156.0

[a]S&W, Smith&Wesson.
[b]Win, Winchester; Rem, Remington; STHP, silver tip hollow point; FMJ, full metal jacket; JHP, jacketed hollow point.
[c]Estimated values at 1 m and at an angle of 90°.

D. Additional measurements

The bullet speed for each weapon and ammunition combination was measured using a PACT model-1 chronograph (Grand Prairie, TX). The chronograph automatically calculated the speed of the bullet as it passed through two light sensors separated by a constant distance. The bullet speed measurements were recorded with the chronograph located 2 m in front of the muzzle. The average speed over five shots for each weapon and ammunition combination is listed in Table II. The peak acoustic SPLs in units of decibels re 20 μPa were recorded using a B&K Type 2230 (SPL) meter. The peak SPL measurements were recorded at 20 m from the source and at 90° to the line-of-fire. A value of 26 dB was added to the SPL measurements in order to obtain the 1 m source SPL estimates listed in Table II. Simultaneous recordings from microphones positioned at multiple distances from the source verified the 6 dB SPL attenuation per doubling the distance.

IV. VARIATIONS IN EMPERICAL FIREARM WAVEFORMS

In this section, waveform signatures are shown to vary due to differences in the source-to-microphone distance and due to changes in the azimuth angle (angle between the line-of-fire and the microphone with the muzzle at the origin). Comparisons are made showing waveform variations among different firearm types, firearm models, barrel lengths, and ammunition types. The correlation coefficient is used to quantify variations between two waveforms.

A. Muzzle blast results for multiple recording distances at a constant angle

The cross-range set of experiments was designed to demonstrate the effects of different microphone distances from the source with the azimuth angle held constant. The following set of plots show the time series pressure waveforms recorded by each of four microphones located at 1.5, 3, 6, and 30 m from the muzzle. Even though the signals were recorded simultaneously, they arrive at each microphone at different times due to different propagation times. In order to compare waveform shapes recorded at different distances, each signal is displayed with the peak of the muzzle blast positioned at the 2 ms time mark.

Figure 6 shows the waveforms recorded at 90° for a 0.38 caliber Smith&Wesson model 10 revolver (Springfield, MA) with a barrel length of 2.5 in. (6.4 cm) and firing a Winchester 110 grain (7.1 g) silver tip hollow point bullet (Table II, index #3). There are three primary acoustic events observable in these waveforms. The largest event is the muzzle blast positioned with its peak at 2 ms. The smaller peak just preceding the muzzle blast is attributed to internal ballistics sounds—gas escaping from the gap between the cylinder and the barrel. The third event is the ground reflection occurring after the muzzle blast.

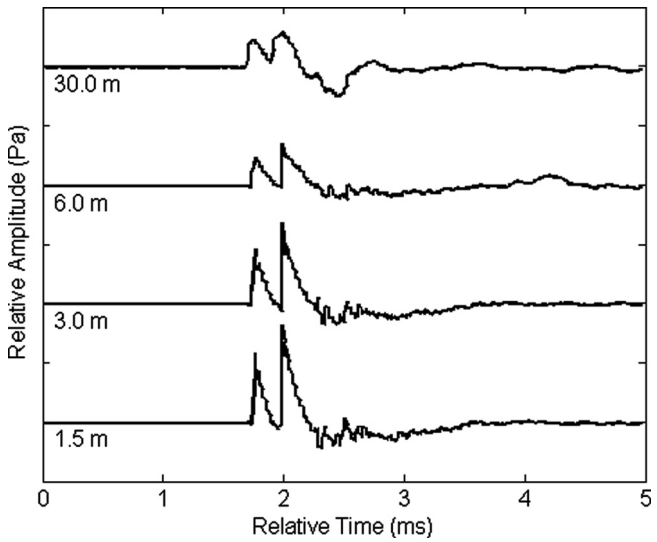

FIG. 6. Simultaneous recordings of waveforms from multiple distances along the 90° azimuth angle for a Smith&Wesson model 10 .38 caliber revolver with a 2.5 in. barrel.

There are several noticeable phenomena taking place at longer ranges. First, the waveform appears smoother at the 30 m range due to molecular absorption of high frequencies. Second, the positive phase duration (measured from the muzzle blast peak to the first zero crossing) increases as the microphone distance increases (0.22 ms at 1.5 m, 0.25 ms at 3.0 m, and 0.26 ms at 6.0 m). An exception occurs at 30 m where the positive phase duration was measured at 0.16 ms—possibly due to transitions from a shock front to a linear wave. The non-linear dispersion effect held for all firearm recordings made at distances of 1.5 to 6.0 m. Finally, the time difference of arrival between the muzzle blast and its ground reflection is greatest for the 1.5 m waveform and becomes shorter as the source-to-microphone distance increases [see Eq. (14)].

Figure 7 shows the recordings made at 90° for the same model 0.38 caliber revolver and same ammunition as shown in Fig. 6, but with a longer (4.0 in./10.3 cm) barrel (index #4). The longer barrel firearm had a higher bullet speed (287 m/s vs 270 m/s) and a lower peak SPL for the muzzle blast (151.4 dB vs 153.0 dB SPL). The longer barrel time accounts for the increased separation between the two peaks in the waveform corresponding to the cylinder gap blast and the muzzle blast. At the 90° azimuth angle, the first peak is higher than the second peak (the muzzle blast), a result that was only observed in recordings from this revolver and for azimuth angles greater or equal to 90°. The muzzle blast waveform was more distorted in the 30 m recording compared to that in Fig. 6. Similar muzzle blast distortions were observed in all 30 m recordings for all firearms.

B. Muzzle blast results for multiple angle recordings at constant range

The cross-angle set of experiments was designed to demonstrate the directional effects of the muzzle blast using multiple microphones at constant range, but located at different azimuth angles with respect to the line-of-fire. Figure 8 shows the time series pressure waveforms recorded by four microphones located along the 30 m arc at 3°, 30°, 60°, and 90° and then at 90°, 120°, 150°, and 180°. The forward and rear configurations, each recorded during separate sessions, were time-aligned according to the highest peak in the cross correlation between the two 90° degree microphones. The waveform from the 3° microphone is positioned at the 2 ms time mark, and the signals from all other microphone locations are displayed relative to that time offset.

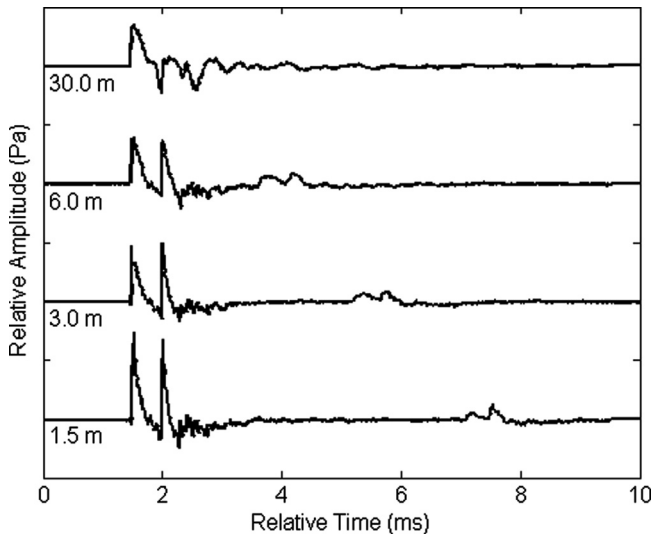

FIG. 7. Simultaneous recordings of waveforms from multiple distances along the 90° azimuth angle for a Smith&Wesson model 10.38 caliber revolver with a 4 in. barrel. The longer barrel revolver has greater separation between the cylinder blast and the muzzle blast.

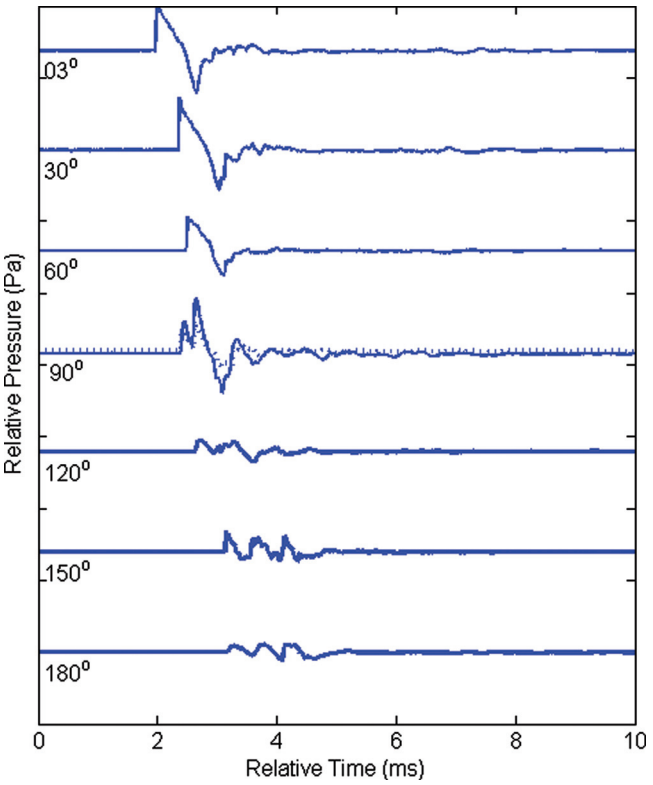

FIG. 8. (Color online) Simultaneous recordings of waveforms from multiple azimuth angles (3°–180°) at a distance of 30 m for a Smith&Wesson model 10.38 caliber revolver with a 2.5 in. barrel.

The waveforms in Fig. 8 result from a 0.38 caliber Smith&Wesson model 10 revolver with a 2.5 in. (6.4 cm) barrel firing a Winchester 110 grain (7.1 g) silver tip hollow point bullet (index #3). The bullet was subsonic, so the acoustic events consist only of internal ballistics sounds, the muzzle blast, and ground reflections. The waveform at 90° is similar to the 30 m waveform shown earlier in Fig. 6. In general, the muzzle blast arrives later in time as the azimuth angle increases because of the smaller blast intensity in those directions. The internal ballistic events have comparatively low intensity and are obscured by the muzzle blast for the recordings at angles 3°, 30°, and 60°. The waveforms recorded at angles of 90° and greater show three distinct events composed of internal ballistic sounds, the muzzle blast, and the ground reflection.

The next three figures show the waveform variations at a constant range of 30 m and at angles 3°–90° for two different revolver models, a revolver and a semi-automatic pistol, and a revolver firing two different weight bullets. Figure 9 shows the cross angle waveforms for a model 10 (index #3)

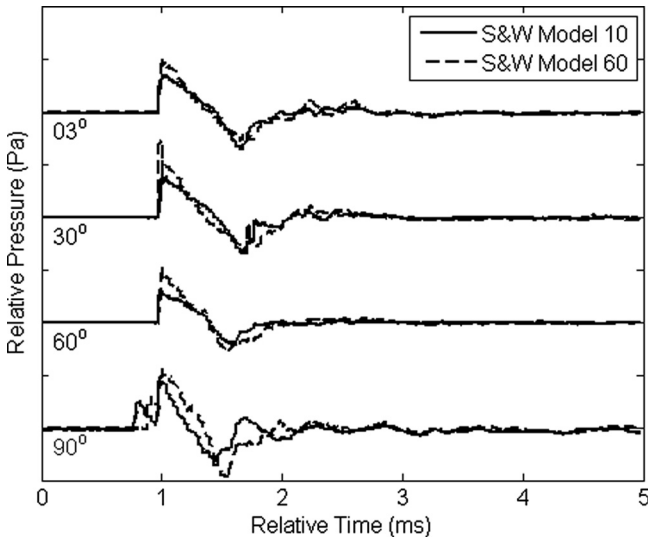

FIG. 9. Recordings of waveforms from multiple azimuth angles (3°–90°) at a distance of 30 m for two different Smith&Wesson revolver models.

and a model 60 (index #5) Smith&Wesson 0.38 revolvers with the same barrel lengths and firing bullets with the same weight. The waveforms from recordings at angles 3°–60° have similar shapes; however, the model 60 waveforms have slightly higher peak levels corresponding to the higher SPL for model 60 listed in Table II (model 10 SPL = 153.0 dB and model 60 SPL = 155.4 dB). The waveforms from the microphone at 90° show a larger lateral blast before the muzzle blast for model 10 compared to the waveform for model 60. This large lateral blast likely accounts for the smaller peak muzzle blast pressures from model 10.

Figure 10 shows the cross angle waveforms for a Smith&Wesson model 10 0.38 revolver (index #4) and a Sig Sauer 9 mm semi-automatic pistol (index #6) (Exeter, NH). These two firearms have similar barrel lengths and similar bullet weights. The waveforms from recordings at angles 3° and 30° have similar shapes, but the pistol has slightly higher peak pressures corresponding to a higher SPL in Table II (revolver SPL = 151.4 dB and pistol SPL=153.7 dB). The revolver waveforms from recordings at angles 60° and 90° have a pronounced lateral blast before the muzzle blast. There are no identifiable acoustic events before the muzzle blast from the pistol.

Figure 11 shows the cross angle waveforms for a Smith&Wesson model 13 0.357 magnum revolver firing ammunition with different bullet weights (index #1 and index #2). These waveforms were recorded at a constant distance of 3 m and provide a clear separation between the muzzle blast and its ground reflection. The lighter bullet was supersonic and the ballistic shockwave is visible in the recording from the 3° recording. The recorded waveform from firing the heavier bullet does not show a ballistic shockwave, but the muzzle blast has a significant distortion, possibly due to a transonic bullet (bullet speed measured at 362 m/s with the speed of sound estimated at 354 m/s). The muzzle blast from firing the lighter bullet had a higher peak SPL compared to that from the heaver bullet (155.4 dB compared to 158.5 dB). The waveforms recorded at 30° and 60° are similar, but the heavier bullet resulted in a larger separation between the muzzle blast and the cylinder blast in the waveform recorded at 90°.

C. Multiple shot cross correlation results

All weapons were fired five times in succession at each microphone configuration. Shot-to-shot variability was measured by computing the pairwise product-moment correlation coefficient between the shots. The correlation coefficient ρ of two variables X and Y is defined as the covariance of X and Y normalized by the product of their individual standard deviations σ_X and σ_Y:

$$\rho = \frac{\mathrm{cov}(X,Y)}{\sigma_X \sigma_Y}. \quad (15)$$

The range of values for the correlation coefficient is $-1 \le \rho \le 1$. If X and Y have a perfect linear relationship,

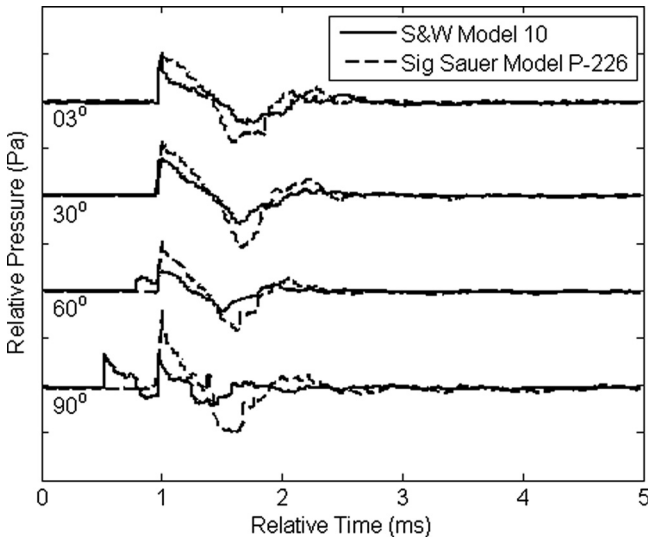

FIG. 10. Recordings of waveforms from multiple azimuth angles (3°–90°) at a distance of 30 m for a revolver and a semi-automatic pistol.

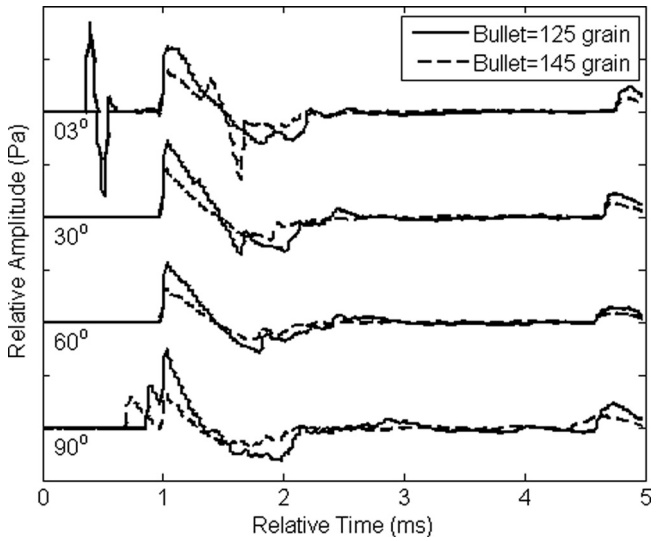

FIG. 11. Recordings of waveforms from multiple azimuth angles (3°–90°) at a distance of 30 m for a revolver firing two different bullet weights.

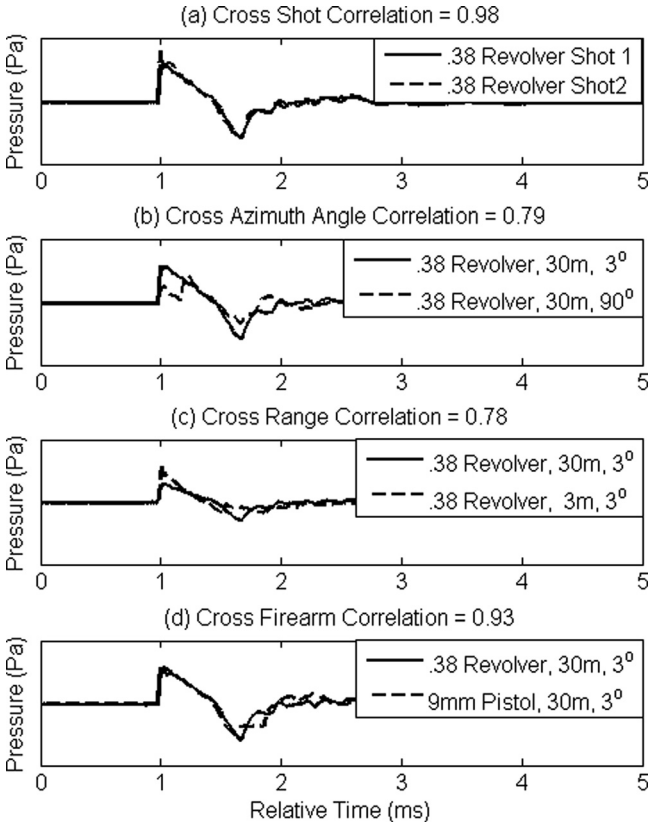

FIG. 12. Correlation results between gunshot waveforms recorded from multiple shots, different azimuth angles, different source-to-microphone distances, and different firearms.

that is $Y = mX + b$, where m ($\neq 0$) and b are constants, then the value of ρ will be ± 1. A value of -1 indicates a perfect linear relationship but with opposite phase. If the two variables are uncorrelated, then ρ will be equal to zero. However, a zero correlation does not imply statistical independence, but rather the lack of a linear relationship. When applied to firearm waveforms, there are two important properties of the product-moment correlation. Since the correlations are based on a normalized covariance, the coefficients are not affected by scale (recorded amplitude) or by a constant amplitude offset.

The firearm waveform under test consisted of a 5 ms segment starting 1 ms before the muzzle blast peak. The reference waveform was a 7 ms segment starting 2 ms before the muzzle blast peak. Correlation coefficients were computed at every sample as the test waveform was slid across the reference waveform for a period of 2 ms. The maximum correlation value was then chosen as the best alignment of the two waveforms and the point with the best linear relationship.

Most successive-shot correlations with source, environment, and receiver variations held constant are very high. The top plot in Fig. 12 shows the first two shots of a subsonic 0.38 revolver (index #3) recorded at a distance of 30 m and at an angle of 3°. The correlation coefficient for these two shots is 0.98.

Correlations between waveforms from different angles and different distances are typically lower than those between successive shots. The second plot from the top in Fig. 12 shows the 30 m waveforms at a 3° and a 90°azimuth angle for the 0.38 revolver (index #3). The correlation coefficient for these two waveforms was 0.79. The third plot shows the 3° azimuth angle waveforms at the 3 and 30 m range for the 0.38 revolver (index #3). The best correlation for these two waveforms was 0.78. Angular dependence of blast size, internal ballistics, non-linear spreading, and ground reflections are all the significant factors contributing to the lower correlation coefficients.

Correlations between waveforms from different firearm types can vary significantly, depending on the size of the blast, the internal ballistics, the azimuth angle, and the sensor distance. The bottom plot shows the waveforms for a 0.38 revolver (index 3#) and a Sig Sauer 9 mm semi-automatic pistol (index #6) recorded at the same distance and angle. The correlation coefficient for these two waveforms from different firearm types is 0.93. These two different firearm types had a higher correlation coefficient that that from two revolvers with different barrel lengths because they had similar muzzle blast sizes, similar bullet speeds, and the recordings were made in the forward direction.

Table III lists correlation coefficients for different firearm conditions including different firearm types, different firearm models, different ammunition weights, and different barrel lengths. Waveforms were selected from recordings made at azimuth angles 3°–90° and at a distance of 30 m. These results show a strong dependence on blast size and azimuth angle, but have higher than expected variability due

TABLE III. Correlation coefficients comparing acoustic gunshot waveforms recorded from different firearm conditions and at multiple azimuth angles (at a distance of 3 m).

Comparison	Table II Indices	Angle 3°	Angle 30°	Angle 60°	Angle 90°
Revolver models	3 vs 5	0.93	0.89	0.95	0.71
Pistol models	6 vs 7	0.80	0.90	0.95	0.87
Rifle models	12 vs 14	0.79	0.91	0.68	0.79
Revolver vs pistol	3 vs 6	0.93	0.93	0.91	0.56
Revolver vs rifle	3 vs 12	0.62	0.62	0.70	0.25
Pistol vs rifle	6 vs 12	0.53	0.46	0.58	0.66
Revolver Ammo Wts.	1 vs 2	0.61	0.95	0.96	0.73
Pistol ammo Wts.	6 vs 10	0.88	0.87	0.85	0.73
Rifle ammo Wts.	12 vs 13	0.95	0.97	0.75	0.94
Revolver barrel length	3 vs 4	0.88	0.94	0.75	0.54

TABLE IV. Estimated muzzle blast exponential decay parameter b for different firearms recorded at multiple microphone azimuth angles (at a distance of 3 m).

Firearm comparison	Table II index	Angle 3°	Angle 30°	Angle 60°	Angle 90°
Revolver	3	0.87	0.88	0.88	0.78
Revolver	4	0.83	0.86	0.76	0.65
Revolver	5	0.88	0.90	0.89	0.81
Pistol	6	0.83	0.85	0.83	0.80
Pistol	7	0.82	0.87	0.85	0.82
Pistol	10	0.78	0.79	0.82	0.78
Rifle	12	0.73	0.98	0.93	0.91
Rifle	13	0.77	0.96	0.92	0.87
Rifle	14	0.86	0.88	0.88	0.90

to the presence/absence of pre-muzzle blast events and the effect of ground reflections superimposed with the muzzle blast waveform.

D. Waveform modeling results

In Sec. II, the Friedlander equation was presented as a model for explosions in air. Eq. (1) is parameterized by the peak overpressure P_s, the positive phase duration T_0, and the exponential rate of decay b. The frequency of the spectrum peak can be computed from the parameters T_0 and b. Estimates of these parameters can be computed using non-linear optimization techniques like the MATLAB function fminsearch that uses the Nelder-Mead simplex method. Estimated values for the parameters T_0 and b for a combination of firearm and ammunition types recorded at 3 m distance (no ground reflection interference) and for four azimuth angles in the forward direction are given in Tables IV and V. From Table IV, the median value for the decay parameter b is 0.83 for handguns and 0.88 for rifles. From Table V, the median value for the positive phase duration T_0 is 0.29 ms for handguns and 0.47 ms for rifles, corresponding to larger median SPL values (153 dB for handguns and 160 dB for rifles). The percent of error between the estimated and the measured parameter T_0 at 3 m distance is 9%. The median value for T_0 at 30 m distance is 0.31 ms for handguns and 0.43 ms for rifles with an overall error of 22%.

TABLE V. Estimated muzzle blast positive phase duration parameter T_0 in milliseconds for different firearms recorded at multiple microphone azimuth angles (at a distance of 3 m).

Firearm comparison	Table II index	Angle 3°	Angle 30°	Angle 60°	Angle 90°
Revolver	3	0.33	0.33	0.33	0.27
Revolver	4	0.33	0.33	0.24	0.17
Revolver	5	0.32	0.32	0.32	0.29
Pistol	6	0.30	0.28	0.25	0.25
Pistol	7	0.31	0.29	0.27	0.25
Pistol	10	0.24	0.25	0.22	0.21
Rifle	12	0.47	0.64	0.52	0.47
Rifle	13	0.57	0.64	0.50	0.46
Rifle	14	0.42	0.38	0.38	0.32

TABLE VI. Measured/estimated muzzle blast spectrum peak frequencies in hertz for different firearms recorded at multiple microphone azimuth angles (at a distance of 3 m).

Firearm comparison	Table II index	Angle 3°	Angle 30°	Angle 60°	Angle 90°
Revolver	3	500/410	500/430	500/430	500/440
Revolver	4	570/360	570/390	570/430	280/520
Revolver	5	570/440	570/430	570/500	570/470
Pistol	6	570/400	570/440	850/440	570/460
Pistol	7	740/260	490/420	490/410	490/520
Pistol	10	490/470	490/400	490/540	740/540
Rifle	12	250/240	250/280	490/310	250/330
Rifle	13	250/260	250/250	250/290	250/330
Rifle	14	490/290	490/310	490/340	490/470

Table VI shows the measured estimated spectral peak frequencies for the 3 m recordings. The measured values were computed from the fast-Fourier transform (FFT) of the waveform starting with the muzzle blast and ending before the ground reflection. The median values the for measured/estimated spectral peak frequencies are 570/433 Hz for handguns and 250/300 Hz for rifles. For comparison, the median measured/estimated values for the 30 m recordings are 850/450 Hz for handguns and 740/360 Hz for rifles, indicating increased distortions at longer distances.

V. SUMMARY AND DISCUSSION

The purpose of this study was to investigate sources of waveform variation in acoustic recordings from small firearms. An experiment was conducted using high-quality recording equipment to demonstrate the acoustical effects of different source characteristics and multiple propagation conditions.

The recorded sound from a firearm discharge was found to consist of multiple acoustic events: the ballistic shockwave, internal gas leaks or ejections, the muzzle blast, and reflections. The primary sound is the muzzle blast that has a distinctive shape characterized by an explosion in air. The size of the blast determines the peak overpressure above ambient air pressure and the positive phase duration of the signal. The blast size depends on the gas pressure remaining in the barrel just prior to the bullet exiting the muzzle and was shown to be affected by the ammunition charge, the bullet weight, the barrel length, and internal gas leaks.

The primary factors found to affect variations in recorded acoustic gunshots were the blast size, the microphone distance from the source, and the azimuth angle with respect to the line-of-fire. The presence of a ballistic shockwave depends on the bullet speed (must be supersonic) and the miss distance to the microphone, and the azimuth angle. Pre-muzzle blast sound events (internal gas leaks) were shown to depend on the firearm, the ammunition, and the recording azimuth angle. The size and relative timing of reflections depend on the reflection coefficient, the distance, and the angle of incidence.

Comparing two acoustic signatures can be accomplished qualitatively by visual comparison or quantitatively by

computing the correlation coefficient. Cross correlation results support the observed variations in firearm recordings resulting from different source characteristics and different propagation conditions. Models of the muzzle blast provide estimates of the positive phase duration and the peak spectral frequency, but many recorded firearm waveforms have multiple interfering sources that distort parameter estimates. In particular, recordings from longer distances may have transonic or acoustic waveforms that no longer match a particular model. Finally, the results of this paper represent almost ideal recording equipment and conditions. Field recordings will likely have lower quality and fewer acoustic details than those presented.

ACKNOWLEDGMENTS

This work was funded under DOJ contract number 94182. We would like to acknowledge the Austin Gun Club for allowing us to exclusive use of their range for this data collection. We would like to thank our shooters Lee Orman, Jim Ryan, and Carson Dayley of the FBI, our field test supervisor David Lockett formerly of BAE Systems, and our data collection supervisor Bobby Martin formerly of BAE Systems. We would like to thank Dr. Joel Kalb, Dr. Georges Garinther, and Dr. James Moreland of the U.S. Army Human Engineering Laboratories at Aberdeen Proving Ground, MD, for advice on microphones and microphone positioning.

[1]E. A. Page and B. Sharkey, "System for reporting gunshots in urban environments," in *Proceedings of the Society of Photo-Optical Instrumentation Engineers (SPIE) Symposium on Public Safety/Law Enforcement Technology* (1995), Vol. 2497, pp. 162–172.

[2]Information on the Shotspotter Gunshot Location System available at http://www.shotspotter.com/solutions/index.html (Last viewed 11/08/2010).

[3]G. L. Duckworth, D. C. Gilbert, and J. E. Barger, "Acoustic counter-sniper system," in *Proceedings of the Society of Photo-Optical Instrumentation Engineers. (SPIE) International Symposium on Enabling Technologies for Law Enforcement and Security* (1996), Vol. 2938, pp. 262–275.

[4]Information on the Vehicle-mounted Acoustic Sniper Detection System available at http://www.bbn.com/products_and_services/boomerang (Last viewed 10/25/2010).

[5]T. Mackinen and P. Pertila, "Shooter localization and bullet trajectory, caliber, and speed estimation based on detected firing sounds," Appl. Acoust. **71**, 902–913 (2010).

[6]G. Simon, M. Maróti, A. Lédeczi, G. Balogh, B. Kysy, A. Nádas, G. Pap, J. Sallai, and K. Frampton, "Sensor network-based countersniper system," in *Proceedings of the Second Association Computing Machinery Conference on Embedded Networked Sensor Systems*, Baltimore, MD (2004), pp. 1–12.

[7]P. Volgyesi, G. Balogh, A. Nadas, C. Nash, and A. Ledeczi, "Shooter localization and weapon classification with soldier-wearable networked sensors," in *Proceeding of the 5th International Conference on Mobile Systems*, San Juan, Puerto Rico, (2007), pp. 113–126.

[8]S. D. Beck, H. Nakasone, and J. T. Kalb, "Forensic models for recorded acoustic gunshot signals (A)," J. Acoust. Soc. Am. **107**, 2829 (2000).

[9]R. C. Maher and S. R. Shaw, "Deciphering gunshot recordings," in *Audio Engineering Society 33rd International Conference: Audio Forensics—Theory and Practice*, Denver, CO, Paper 2 (June 2008).

[10]B. E. Koenig, S. M. Hoffman, H. Nakasone, and S. D. Beck, "Signal convolution of recorded free-field gunshot sounds," J. Audio Eng. Soc., **46** (7/8), 634–653 (1998).

[11]H. Krier and M. Summerfield, "Progress in astronautics and aeronautics," *Interior Ballistics of Guns*, American Institute of Aeronautics and Astronautics, New York University, New York, NY, Vol. 66, Part I (1960).

[12]W. E. Baker, *Explosions in Air* (University of Texas Press, Austin TX, 1973), Chap. 1–3.

[13]A. V. Oppenheim, A. S. Willsky, and S. H. Nawab, *Signals and Systems* (Prentice Hall Englewood Cliffs, NJ, 1997), p. 329.

[14]ANSI S2.20-1983: *American National Standard for Estimating Airblast Characteristics for Single Point Explosions in Air* (Acoustical Society of America, New York, 1983).

[15]R. D. Ford, D. J. Saunders, and G. Kerry, "The acoustic pressure waveform from small unconfined charges of plastic explosive," J. Acoust. Soc. Am. **94**, 408–417 (1993).

[16]T. F. W. Embleton, "Tutorial on sound propagation outdoors," J. Acoust. Soc. Am. **100**, 31–48 (1996).

[17]K. Attenborough, S. Taherzadeh, H. E. Bass, X. Di, R. Raspet, G. R. Becker, A. Güdesen, A. Chrestman, G. A. Daigle, A. L'Espérance, Y. Gabillet, K. E. Gilbert, Y. L. Li, M. J. White, P. Naz, J. M. Noble, and H. A. J. M. van Hoof, "Benchmark cases for outdoor sound propagation models," J. Acoust. Soc. Am. **97**(1), 173–191 (1995).

[18]R. T. Beyer, *Nonlinear Acoustics* (Acoustical Society of America, New York, 1997), Chap. IV.

[19]A. A. Atchley, "Not your ordinary sound experience: A nonlinear-acoustics primer," Acoust. Today **1**, 19–24 (2005).

[20]G. R. Garinther and J. B. Moreland, "Transducer techniques for measuring the effect of small-arms noise on hearing," *ARL-TR 11-65*, U.S. Army Human Engineering Laboratories, Aberdeen Proving Grounds, MD (1965) (NTIS AD806921).